Experimental thick-target bremsstrahlung spectra from electrons in the range 10 to 30 keV[†]

J. G. Chervenak and A. Liuzzi

Lowell Technological Institute, Lowell, Massachusetts 01854

(Received 10 June 1974; revised manuscript received 30 January 1975)

The x-ray spectra produced by the bombardment of thick targets with monoenergetic electrons between 10 and 30 keV have been determined as a function of the incident and emission angles. Spectra have been obtained for Al, Cu, Mo, and W using a Si(Li) detector. The electron current absorbed in the target was measured and corrected for backscattering, allowing a determination of absolute x-ray emission. A modified least-squares procedure was used to represent the spectra as analytical functions while taking into account the efficiency and resolution of the detector. The spectra show the effects of both target absorption and angular distribution of the thin-target bremsstrahlung production. Agreement with the Kramers formula is only moderate.

I. INTRODUCTION

The bremsstrahlung spectra produced by the electron bombardment of thick targets are important to an understanding of the process of penetration of electrons through matter. They are also of practical interest because of the widespread experimental and commercial use of x rays and electron beams. X-ray spectra from medical x-ray units and from commercial x-ray tubes have been reported in the literature, but comparison of such spectra to theoretical models of thick-target bremsstrahlung production is hindered by the large inherent filtration and fixed angles. Also, much of the previously reported data was taken with detectors that have much lower resolution than the solid-state detectors that have become available in recent years. Two recent publications serve as a summary of the experimental data.[1,2]

In this paper we report on the thick-target-bremsstrahlung spectra from pure targets of Al, Cu, Mo, and W produced by monoenergetic electrons having energy in the range from 10 to 30 keV. Spectra were determined by correcting data obtained with a Si(Li) detector and a special experimental apparatus which allowed the variation of both the angle of incidence of the electrons and the viewing angle of the detector.

II. EXPERIMENTAL

A schematic diagram of the experimental arrangement, showing the definitions of the angles, is given in Fig. 1. The electron beam is produced by a modified 5AZ television projection tube gun with the acceleration voltage supplied by a low-ripple, highly regulated power supply. The focal spot of the electron beam on the target is about 1 mm in diameter at normal incidence. The electron gun and target are housed in an all-metal oil-less vacuum system maintained at 10^{-6} Torr. Both the gun and targets are mounted such that they can be rotated from outside the vacuum chamber.

The 3-mm-thick liquid-nitrogen-cooled Si(Li) detector has a 30-mm² circular active area arranged normal to the beam and is separated from the main vacuum chamber by a single 2-mil beryllium window as shown in Fig. 1. The collimator shown in Fig. 1 was used to prevent photons scattered off the walls of the vacuum chamber from reaching the detector. The aperture of the collimator was large enough to produce a beam which projects to an area which is larger than, but includes, the active surface of the detector. Thus the solid angle intercepted by the detector was not determined by collimation but was determined by the active area of the detector and distance to the target to be 1.8×10^{-4} sr. A comparison of a spectrum from the uncollimated detector and one from a beam collimated to have a diameter of approxi-
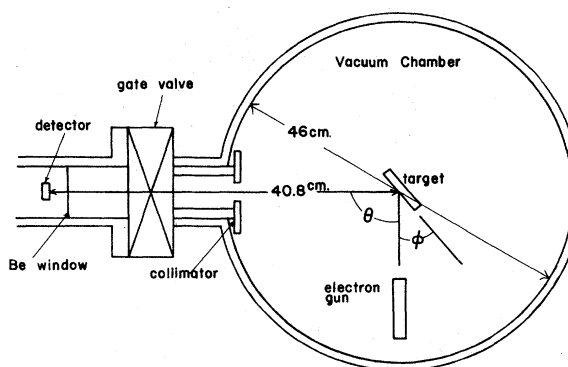

FIG. 1. Schematic diagram of the experimental arrangement showing the definitions of the incident and emission angles. If the outgoing ray lies between the target surface and the incoming electron beam, the angle θ is taken to be negative.

mately 2 mm at the center of the detector surface showed no difference in the shape of the spectrum.

The detector efficiency was calculated from attenuation coefficients and thicknesses of the window, dead layer, and detector. The photo-electric cross section in Si is dominant up to 30 keV, and the reduction in the efficiency due to the scattering of photons out of the sides of the active volume before they have a chance to undergo a photoelectric event is estimated to be less than 1%. The efficiency was found to increase from 28% at 2 keV to 100% at 11 keV, constant at 100% between 11 and 16 keV, and decreased to 50% at 30 keV. The detector system, which exhibits a resolution (FWHM) of 230 eV at 6.4 keV, was cali-brated for energy and checked for linearity using monoenergetic γ and x-ray lines from radioactive sources.

The incident electron-beam current was obtained from the charge absorbed in the target by correct-ing for electron backscattering. The absorbed charge was measured using a current digitizer and scalar with the conventional positive 50-V bias on the target to prevent the loss of secondary elec-trons. Although the bias prevents the escape of the low-energy secondaries, high-energy elec-trons will be backscattered out of the target. The fraction of the electrons backscattered from the target material was measured by alternately mea-suring the current from a Faraday cup and from the target at various angles of electron incidence.

The targets consist of one or more smooth sheets of high-purity metals. Absence of impurities is verified by the absence of foreign characteristic lines in the x-ray spectra. The x-ray pulse-height distributions were collected in a multichannel anal-yzer and subsequently stored on paper tape.

III. DATA

X-ray pulse-height distributions were collected for all the targets at electron energies of 10, 15, 20, 25, and 30 keV. At each energy, the angle of incidence and detector angle were varied in steps of 20° for a total of 36 angular combinations as listed in Table I. An example of a typical pulse-height distribution is shown in Fig. 2(a). All the

TABLE I. Values of angles for which spectra have been determined. See Fig. 1 for definition of ϕ and θ.

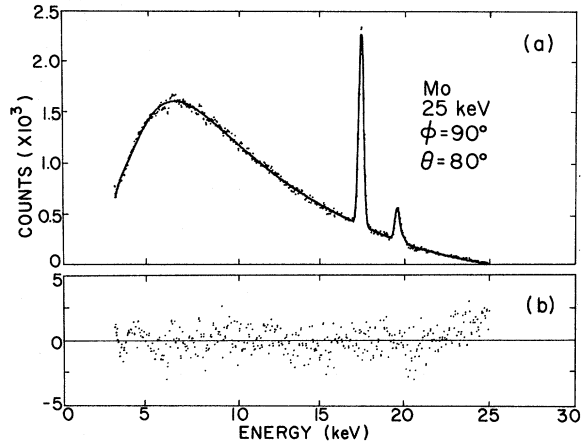| ϕ (deg)	θ (deg)								
90	20	40	60	80					
70	−60	−40	−20	20	40	60	80	100	
50	−40	−20	20	40	60	80	100	120	
30	−20	20	40	60	80	100	120	140	
10	20	40	60	80	100	120	140	160	

FIG. 2. (a) A typical pulse-height distribution. The solid line was obtained from a least-squares procedure. (b) The corresponding normalized residuals defined by $(y_i - Dx_i)/\sqrt{y_i}$.

pulse-height distributions were acquired for ten minutes at a rate of approximately 1000 counts per second. The approximate range of the beam cur-rent was 1–10 nA, and the width of a channel was a nominal 50 eV. A target thickness sufficient to absorb all the x rays produced in the forward direction was used for all the elements except aluminum. For aluminum the magnitude and shape of the continuum did not change in increasing the thickness from 0.25 to 2.03 mm. Thus, all the pulse-height distributions correspond to infinitely thick targets.

IV. DATA ANALYSIS

The experimental data consist of the pulse-height distributions which result when the x-ray spectra emitted from the target are modified by the efficiency and resolution of the detector sys-tem. If both the pulse-height distribution and spec-trum are considered as vectors, then the detec-tor's modification is a linear transformation be-tween them. If D represents the detector response matrix determined by efficiency and resolution and x and y represent the spectrum and pulse-height distribution respectively, then

$$y = Dx. \tag{1}$$

This equation applies to spectra containing both continua and characteristic lines.

Since it was desired to represent the continuum spectrum by a smooth analytical function, a direct inversion of Eq. (1) was not attempted. Instead, the smoothed x-ray spectrum x' was written as a sum of analytical functions for the continua and δ functions for the characteristic lines:

$$x'_i = \sum_j c_j F_j(k_i). \tag{2}$$

The c_j's are arbitrary parameters and $F_j(k_i)$ is the jth function evaluated at the energy of the ith component of the spectrum. Equation (2) can be written in matrix form as

$$x' = Fc. \tag{3}$$

The parameter vector c is determined by fitting the smoothed pulse-height distribution Dx' to the experimental pulse-height distribution y. The least-squares criterion minimizes the Euclidean norm of the difference vector, i.e.,

$$\|y - Dx'\| = \min. \tag{4}$$

Using Eq. (3) and the definition $B \equiv DF$, the equation for c becomes

$$\|y - Bc\| = \min. \tag{5}$$

Equation (5) differs from the usual least-squares equation only in that the F matrix is modified by the detector's response matrix before the least-squares procedure is carried out. In order to perform a weighted fit, each component of the difference vector in Eq. (5) was divided by $\sqrt{y_i}$ before minimization.

The functions that were used to represent the continuum are

$$F_j(k_i) = (E_0 - k_i)/k_i^j, \quad j = 1, 2, \ldots, \tag{6}$$

where E_0 is the incident energy of the electrons. F_1 is equivalent to Kramers' formula for thick-target bremsstrahlung. A separate set of parameters was used for the continuum above and below the absorption edge. Values of j as high as 5 were used for some of the spectra.

The detector response matrix D is the product of a diagonal efficiency matrix D_1 and a resolution matrix D_2. The efficiency was calculated from known absorption coefficients and thickness of the beryllium window, detector, and dead layer. The resolution was assumed to transform a monoenergetic x-ray line into a Gaussian peak with a width parameter $\sigma(E)$. The function $\sigma(E)$ was determined from x- and γ-ray lines from radioactive sources.

The formal solution in Eq. (5) is given by the normal equations

$$c = (\tilde{B}B)^{-1} \tilde{B}y. \tag{7}$$

However, the matrix $\tilde{B}B$ is often ill conditioned and difficult to invert. An alternate method of solution of Eq. (5) due to Golub[3] was used here.

If there are no characteristic lines in the spectrum, the B matrix can be evaluated and a single solution of Eq. (5) will determine the parameter vector. When lines are present, it is necessary to vary the positions and widths of the peaks in order to obtain a good fit. Since the positions and

widths of the peaks are not linear parameters, but enter directly into the calculation of the B matrix, an iterative procedure is necessary. Initial values of the nonlinear parameters are found by quadratic interpolation. The method of minimizing a function without calculating derivatives due to Powell[4] was used to find the over-all minimum in Eq. (5).

χ^2 per degree of freedom and plots of the normalized residuals were used to judge the closeness of fit. The standard deviation in the least-squares parameters are found from the variance-covariance matrix $\Sigma = (\tilde{B}B)^{-1}$. Of more interest is the standard deviation of each point in the spectrum, which is found from the transformed variance-covariance matrix $F\Sigma\tilde{F}$. An over-all measure of the accuracy to which a spectrum is determined was obtained by first setting up a band of height two standard deviations around the spectrum. The ratio of the area of the band to the area under the spectrum was approximately 1% for all of the spectra, indicating that the spectra are known to this accuracy.

The solid curve of Fig. 2(a) is the smoothed pulse-height distribution found from Dx. The adequacy of the fit in Fig. 2(a) can be judged better by examination of the normalized residuals shown in Fig. 2(b). The uniform distribution of the residuals about zero shows the closeness of fit. The χ^2 per degree of freedom, both for the data of Fig. 2(a) and averaged over all the spectra is 1.1. Figure 3 shows an example of the data, smoothed pulse-height distribution, and x-ray spectrum for aluminum. The x-ray spectra differ from the pulse-height distributions mainly at low and high energy and at the absorption edges and characteristic lines.

For molybdenum, the separation of the K_{β_1} and K_{β_2} lines is large enough to require the use of a doublet to obtain a good fit. For tungsten, four L lines were present; two were treated as doublets
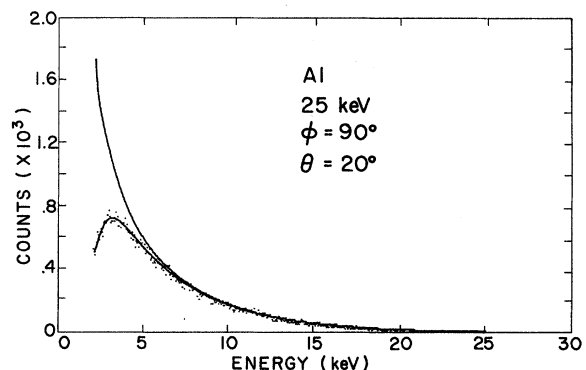

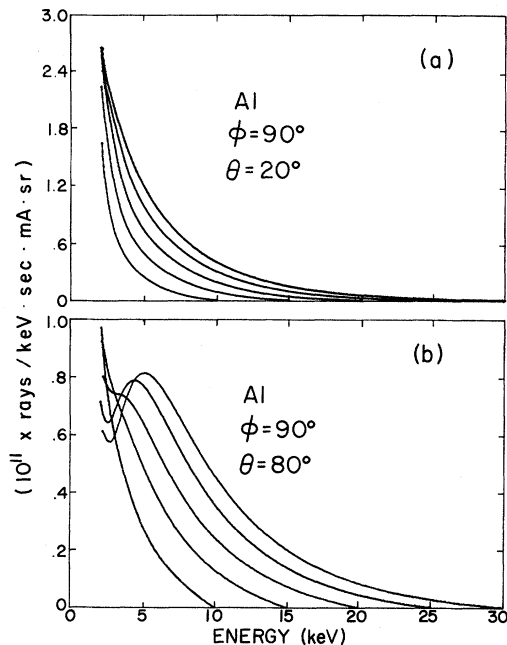FIG. 3. Example of an aluminum pulse-height distribution and spectrum.

FIG. 4. Aluminum spectra at electron incident energies of 10, 15, 20, 25, and 30 keV. (a) Small target absorption. (b) Large target absorption is shown by the decreased emission at low energy.

and two as singlets. There are three L absorption edges for tungsten, but our resolution did not warrant the inclusion of all three in the model, and only the largest edge at 10.198 keV was used. In all the spectra the position of the absorption edges were not determined from the pulse-height distributions but were assumed to be at their known energy. In order to avoid including low-energy characteristic lines in the analysis, the analysis was started at 2 keV for Al, at 3 keV for Cu and Mo, and at 4 keV for W.

V. RESULTS AND DISCUSSION

The least-squares parameters from which all 720 spectra can be easily generated are available from the authors.[5] Only a few of the spectra can be presented here. In Fig. 4(a) are shown the aluminum spectra for five electron energies at a fixed set of angles. The spectra are expressed in terms of the number of x rays within a 1-keV interval that are emitted from the target per time per incident electron current into unit solid angle.

The most noticeable change in the shape of the spectra with angle is due to absorption of the x rays in the target. The absorption is greater for deeper penetration of the electrons (more normal incidence) and for emission at shallow angles where the path lengths (on the average) of the x rays in the target are longer. The spectra of Fig. 4(b) are

viewed at 10° from the target surface, and the x-ray emission at low energy has been greatly reduced due to the absorption. The higher the incident energy, the longer the range of the electrons, and thus the greater is the absorption. At very low energy (about 3 keV), the Al spectra start to increase indicating that at this energy the bremsstrahlung production rate is increasing very rapidly with decrease in energy; this effect was not studied in other elements since the data analysis was not carried to low enough energy due to complex characteristic structure.

The absorption effect is shown for copper in Fig. 5. When the x rays have a large path length in the target as in Fig. 5(b), not only do the spectra turn downward at low energy, but also the size of the discontinuity at the K absorption edge is greatly increased. Again, the absorption is most pronounced at 30 keV.

The Mo and W spectra exhibit the same general angular variation as the lower-Z materials. Figure 6 shows all four elements at the same angles and energy. The tungsten L and copper K edges are seen, but the molybdenum K edge is at high enough energy (20.002 keV) that it is seen only in spectra at the very shallow angles. In this case, and at other angles and energies, the molybdenum spectra have a greater tendency to decrease at low energy than spectra for the elements of higher or lower Z.
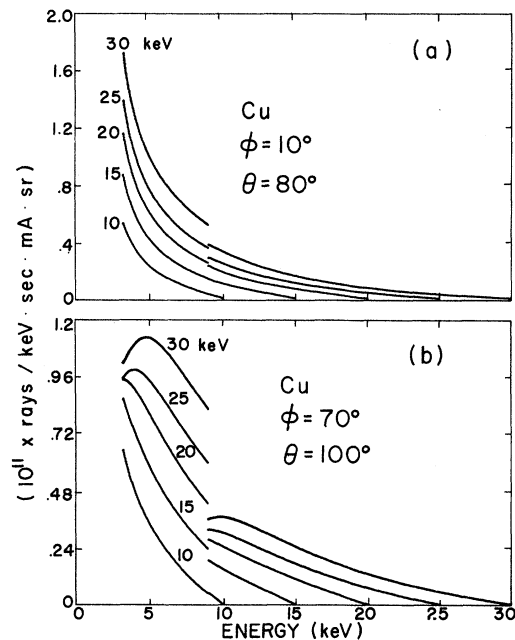

FIG. 5. Copper spectra. (a) Angles producing minimal target absorption. (b) Large target absorption with resulting large discontinuities at the absorption edge.
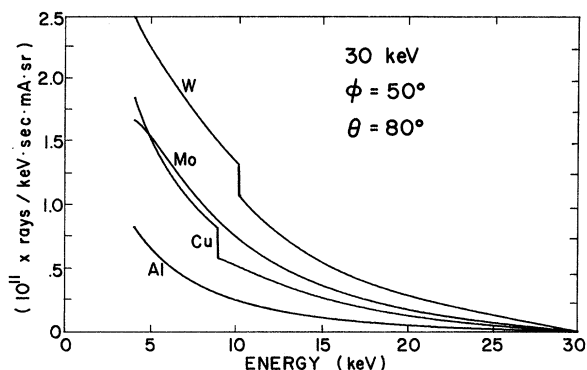
FIG. 6. Comparison of spectra from different elements.

The angular distribution of the thick-target bremsstrahlung depends strongly on the energy of the emitted x rays. The number of x rays emitted in an interval about the energies 5, 15, and 25 keV due to normally incident electrons of 30 keV are shown for Al and W in Fig. 7. All the curves have been drawn to have about the same area; the magnitude of the emission is, of course, much smaller for 25 keV than for 5 keV as is seen in Fig. 6. The shape of the curve at 5 keV shows the target absorption at angles close to the target surface. However, for higher-energy x rays, emission is greater at shallow angles than normal to the target. In the high-energy tail of the spectra,
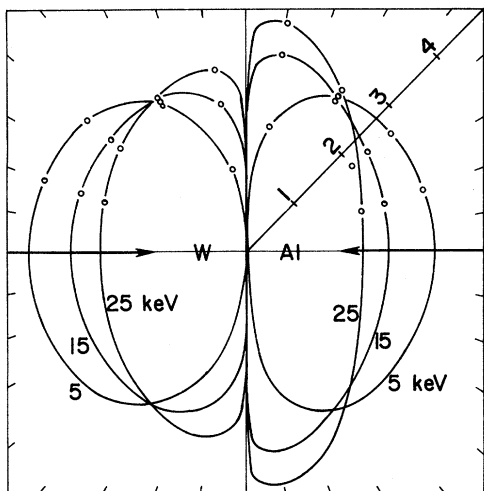

FIG. 7. Normalized distribution of the bremsstrahlung at 5, 15, and 25 keV due to 30-keV electrons at normal incidence. The radial units vary from curve to curve. The value of a radial unit in x rays/keV sec mA sr is: Al at 5 keV, 4.4×10^{10}; at 15 keV, 7.0×10^9; at 25 keV, 8.6×10^8; W at 5 keV, 1.5×10^{11}; at 15 keV, 4.1×10^{10}; at 25 keV, 9.5×10^9. For W, the electrons are incident from the left; for Al, from the right. Data were taken only on one side of the incident beam, and the lower half of the figure is the reflection of the upper half.
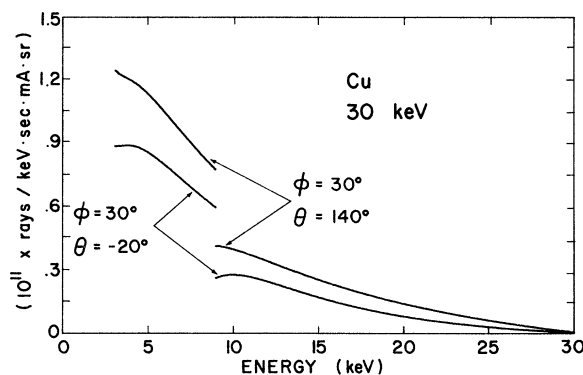

FIG. 8. Two spectra with the same amount of target absorption.

the increased absorption at shallow angles is more than offset by the increased emission at 90° to the beam. The effect is much greater in the low-Z than in the high-Z material.

At certain sets of incident and emergent angles, such as $\phi = 30°$, $\theta = -20°$ and $\phi = 30°$, $\theta = 140°$, the average x-ray path lengths in the target are equal (on the assumption that the target-detector distance is much larger than the diameter of the electron beam's focal spot on the target). The difference in spectra taken at two such sets of angles is not due to target absorption, but only to the angular dependence of the thin-target bremsstrahlung production. The two copper spectra in Fig. 8 show that there is a greater thick-target bremsstrahlung production in the forward direction at all x-ray energies. This effect is also seen in the spectra from the other elements. The copper K_α and K_β characteristic radiation, which is emitted isotropically in the target, has the same magnitude to within 4% for the two spectra of Fig. 8. Also, the size of the discontinuity at the K absorption edge is seen to be very nearly the same for these spectra as is expected.

The distribution of the total number of continuum x rays emitted from a copper target (the area under a spectrum from 3 to 30 keV) as a function of the angle of emission at various angles of electron incidence is shown in Fig. 9. The angular distribution becomes progressively more asymmetrical as the electron beam becomes more oblique to the target. At $\phi = 10°$, the distribution is markedly peaked in the forward direction—the total emission at $\theta = 160°$ is larger than at $\theta = 80°$ even though the target absorption is much greater.

VI. COMPARISON

There is very little experimental data in the literature to which a comparison of these x-ray spectra can be made. Because of the great choice
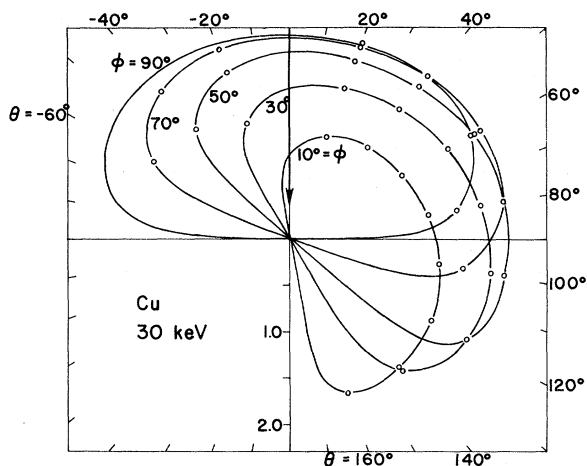
FIG. 9. Angular distribution of total number of continuum x rays. The electrons are always incident from the top of the figure. The target orientation rotates clockwise as the electron beam becomes more oblique to the target surface. The radial units are 10^{12} x rays/mA sec sr.

of experimental conditions, i.e., energy of the electrons and angles of emission and incidence, very little data overlap that presented here. The spectra that are most comparable are those of Unsworth and Greening.[6] Figure 10 shows the 30-keV tungsten spectrum of Unsworth and Greening as presented by Storm[1] along with the spectrum from this work which most closely corresponds in
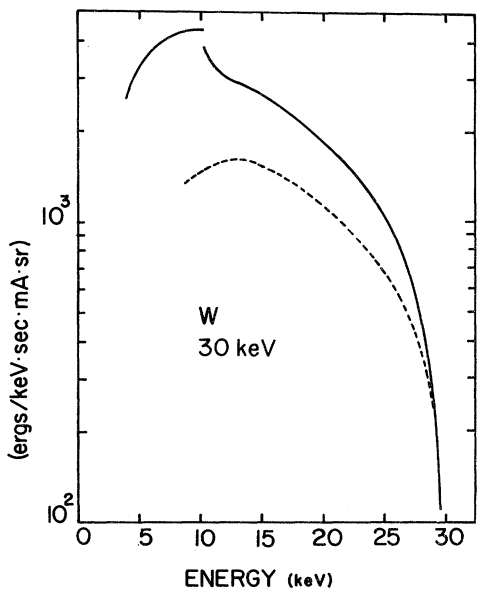
angles. The slight difference in angles probably accounts only for a small amount of the difference between the two spectra. The shapes of the spectra are consistent when the much lower resolution detector used by Unsworth and Greening is considered.

The most often used theoretical thick-target bremsstrahlung formula is that due to Kramers.[7] Kramers' formula can be derived by assuming that the thin-target bremsstrahlung is proportional to Z^2/E (not a function of the x-ray energy k) and that the energy loss $-dE/ds$ is proportional to Z/E (the Thompson-Whiddington law). Using the continuously slowing down approximation, an integration over the paths of the electrons yields the thick-target formula for the x-ray energy emitted from the target

$$I_{E_0,k} = KZ(E_0 - k), \qquad (8)$$

where K is a constant.

Storm used numerical integration to derive thick-target spectra from various thin-target formulas and compared them to tungsten spectra mainly from x-ray tubes.[1] Storm used the Bethe energy-loss equation and corrected the spectra for target absorption and electron backscattering losses. Neither Kramers' or Storm's treatment used a thin-target formula that was differential in angle as well as energy. Thus, in the theoretical spectra, the angular dependence of the thin-target bremsstrahlung has been removed by integration.

Equation (8) predicts that the thick-target bremsstrahlung spectra expressed in terms of emitted energy will be straight lines. Since Kramers' formula does not take into account target absorption, comparison is most meaningful when absorption is least as in the spectra of Fig. 11. Only above $\frac{1}{2}E_0$ do the spectra resemble straight lines. The increased slope of the W spectrum near the high-energy cutoff was first reported by Kuhlenkampff.[8]
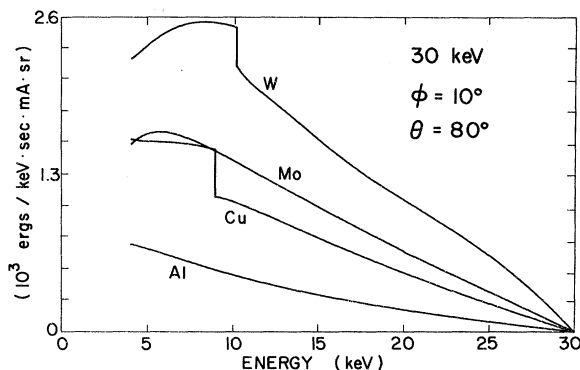

FIG. 10. Comparison of 30-keV tungsten spectra from Unsworth and Greening (dashed line) at $\phi = 70°$, $\theta = 90°$ to this work (solid line) at $\phi = 70°$, $\theta = 80°$.

FIG. 11. Spectra expressed in terms of emitted energy. Kramers' formula predicts straight lines.

Unsworth and Greening[9] modified Kramers' formula to include absorption in the target. In order to properly account for attenuation, it is necessary to know the depth distribution of the electrons as a function of their residual energy. Instead, Unsworth and Greening assume that all the electrons of a given energy can be considered to be at the same depth in the target. Kramers' formula modified using this assumption is compared to a copper spectrum in Fig. 12. Rather than dividing the energy interval into five parts as was done by Unsworth and Greening, numerical integration was used with a 600-eV step size. Also, instead of assuming that the electrons penetrate straight into the target, the average depth in the target was taken from a Monte Carlo calculation by Bishop.[10]

The modified Kramers formula has not been corrected for electrons lost from the target due to backscattering. A method for correcting Kramers' formula for backscattering has been given by Storm[1]; however, it depends on the use of experimental data for the energy distribution of the backscattered electrons. The data that Storm used were for angles of incidence different from that of Fig. 12 so that his correction curve cannot be directly applied to Fig. 12. Qualitatively, however, it is expected that the effect of neglecting backscattering is to overestimate the number of low-energy x rays as indicated by Storm's Fig. 3.

In order to plot the curve of Fig. 12, the constant K in Kramers' formula was evaluated by requiring that both Kramers' and the experimental spectra give the same total number of x rays. Above the absorption edge, the two spectra have roughly the same shape. The smaller discontinuity in the modified Kramers formula is qualitatively expected because the assumption of Unsworth and Greening does not give enough weight to the absorption of x rays produced by electrons which are
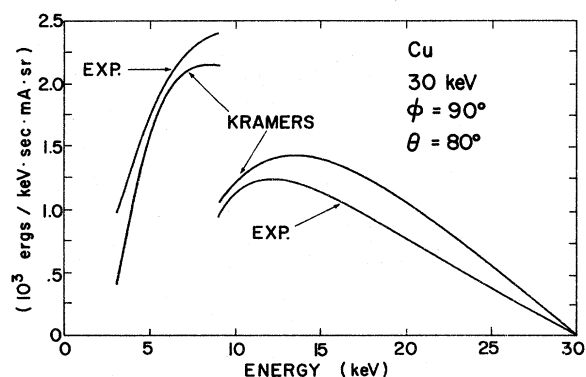
of greater than average depth in the target. The underestimate given by the modified Kramers formula at low energies would be even greater if backscattering had been taken into account.

Equation (8) also predicts a linear increase in x-ray production with atomic number. To check this, the experimental spectra were integrated from $\frac{1}{2}E_0$ to E_0 (the range in which they are roughly linear) and plotted in Fig. 13. If Eq. (8) is integrated over the same limits, the expression $(\frac{1}{8}KE_0^2)Z$ is obtained. The straight lines of Fig. 13 are least-squares fits to this expression and the resultant values of K are given in the caption. The linear increase with Z obviously is not valid for aluminum except for very low values of E_0. Also, the monotonic decrease of K with increase of E_0 shows that K is really not a constant independent of E_0.

VII. CONCLUSIONS

In the analysis it was shown that the statistical uncertainty in the spectra is about 1%, and it is felt that the detector's efficiency is also known to within a few percent. The correction for the resolution of the detector is small and not expected to contribute much to the uncertainty of the spectra even near the characteristic lines and the absorp-
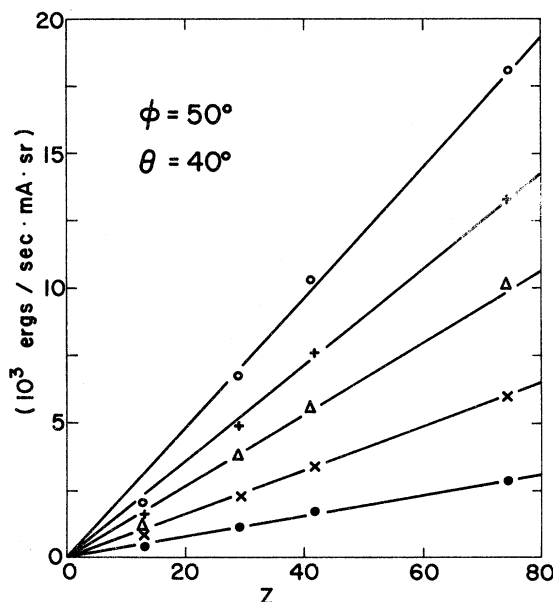
FIG. 12. Comparison to Kramers' formula modified for target absorption.

FIG. 13. X-ray emission as a function of atomic number. The ordinate is the energy emitted between $\frac{1}{2}E_0$ and E_0. The straight lines are least-squares fits to the prediction of Kramers' formula. ●: $E_0 = 10$ keV, $K = 3.08$; ×: $E_0 = 15$ keV, $K = 2.89$; △: $E_0 = 20$ keV, $K = 2.67$; +: $E_0 = 25$ keV, $K = 2.29$; ○: $E_0 = 30$ keV, $K = 2.15$.

tion edges although this source of error is hard to estimate quantitatively. The power supply voltage and the energy calibration of the detector system were individually made to within 0.1% and were jointly verified to within 1% by the high-energy cutoff of the spectra. The alignment of the targets in the holder was checked by the symmetry of the backscattering fractions, and it is felt that the angle was set accurately to within less than 1°. At shallow angles of incidence (small values of ϕ) the 1° incertainty could lead in the worst case (Al, $\phi = 10°$) to an uncertainty of 5% in the backscattering fraction. Since the incident-electron current is determined using the backscattering fraction, an error of up to 5% in the absolute intensity could result. In all, it is felt that absolute spectra have been determined with an uncertainty of 5–15%.

An experimental description of thick-target bremsstrahlung spectra as a function of angle, energy, and atomic number has been presented.

The connection between these thick-target spectra and thin-target bremsstrahlung formulas requires a comprehensive theory of the passage of electrons through matter. In particular, the correction for the absorption in the target requires a knowledge of the depth distribution of the electrons as a function of their residual energy. It was also shown that the angular distribution of the thick-target bremsstrahlung found here can only be explained by the use of a thin-target formula which is differential in angle as well as energy.

While Kramers' formula serves as a useful, approximate description of thick-target bremsstrahlung, close examination of the experimental data shows many areas of disagreement. Even for x-ray energies large enough that target absorption is negligible, the spectra can be only roughly described as straight lines. Also, the predicted dependence of the emission on incident energy and atomic number was not verified.

---

[1]E. Storm, Phys. Rev. A 5, 2328 (1972).
[2]J. R. Greening, in *Topics in Radiation Dosimetry*, edited by F. H. Attix (Academic, New York, 1972), p. 262.
[3]G. Golub, Numer. Math. 3, 206 (1965).
[4]M. J. D. Powell, Comput. J. 7, 155 (1964).
[5]Address inquiries for spectra not presented here to

A. Liuzzi, Department of Radiological Sciences, Lowell Technological Institute, Lowell, Mass. 01854.
[6]M. H. Unsworth and J. R. Greening, Phys. Med. Biol. 15, 631 (1970).
[7]H. A. Kramers, Philos. Mag. 46, 836 (1923).
[8]H. Kuhlenkampff, Ann. Phys. (Leipz.) 69, 548 (1922).
[9]M. H. Unsworth and J. R. Greening, Phys. Med. Biol. 15, 621 (1970).
[10]H. E. Bishop, Br. J. Appl. Phys. 18, 703 (1967).